Towards the chiral limit with dynamical blocked Wilson fermions

I. Barbour
Department of Physics and Astronomy, University of Glasgow, Glasgow G12 8QQ, United Kingdom

E. Laermann
Höchstleistungsrechenzentrum HLRZ, c/o Kernforschungsanlage Jülich G.m.b.H., Postfach 1913, D-5170 Jülich, Federal Republic of Germany

Th. Lippert and K. Schilling
Fachbereich Physik, Universität Wuppertal, Gaussstrasse 20, 5600 Wuppertal 1, Federal Republic of Germany
(Received 13 April 1992)

The approach to the chiral limit in full QCD is investigated with a blocked Wilson fermionic action. Finite size effects prohibit taking the chiral limit on small lattices. We find that various observables expected to be influenced by chiral and finite temperature properties of the theory reveal patterns which suggest a transition to chiral-symmetry restoration and deconfinement to be the origin of the observed phenomena.

PACS number(s): 12.38.Gc, 11.15.Ha, 12.38.Aw

I. INTRODUCTION

Wilson's formulation of (full) quantum chromodynamics (QCD) on a lattice breaks chiral symmetry explicitly and therefore requires careful preparatory work to show that it is a meaningful discretization of QCD. In order to perform the proper continuum limit, it is mandatory to establish the existence of a chiral limit at which the dynamics of the theory is chirally symmetric. At this value of the hopping parameter, the symmetry of the ground state is expected to be spontaneously broken, leading to a massless Goldstone boson, the pion. In the quenched approximation, the determination of the chiral limit is achieved by varying the valence quark hopping parameter $\kappa^{(\mathrm{val})}$ towards its critical value $\kappa_c^{(\mathrm{val})}$ where the pion mass vanishes. This is done configuration by configuration on a quenched equilibrium ensemble. On a finite lattice the value of $\kappa_c^{(\mathrm{val})}$ fluctuates among different equilibrium configurations and one usually quotes the average of the distribution as the "critical value."

When the dynamics of quarks is taken into account, the approach to κ_c becomes much more involved because the quarks now play an active role in the updating procedure. One has to vary the hopping parameter of the dynamical quarks κ and tune it towards its critical value. Thus, a variety of equilibrium gauge field ensembles at κ values increasingly closer to the expected chiral limit has to be generated. Clearly, as it is the case in quenched QCD for $\kappa_c^{(\mathrm{val})}$, one cannot reach κ_c, because the fermionic matrix acquires a zero mode in this limit and renders the application of linear equation solvers utterly inefficient. In order to determine the location of κ_c, one has to perform an extrapolation of a suitable observable from the generated set of κ values. For example, one could study the eigenvalue spectrum of the fermion matrix and extrapolate the lowest eigenvalue, as a function of κ, to zero. The nice feature of this method is that, in principle, it allows one, for any given configuration, to determine the critical valence $\kappa_c^{(\mathrm{val})}$ of that configuration without having to introduce and actually tune a valence quark hopping parameter. However, the computation of the spectral distribution for Wilson fermions is very memory consuming and thus so far only applicable for small lattices.

Such a procedure to approach the chiral limit of full QCD is hampered by a problem observed some time ago by Fukugita, Ohta, and Ukawa [1]. On a $5^3\times 3$ lattice, it turned out that, unlike in quenched QCD, it was not possible to successively increase κ close towards its critical value. At some values way before the chiral limit was reached, a qualitatively new behavior sets in resembling features of a deconfinement transition. This behavior was confirmed in a further study [2] which suggested finite size effects triggered by a deconfinement mechanism as an explanation. As such, the occurrence of finite size effects as the quark mass is lowered is not surprising. At increasingly smaller quark masses, virtual pion loops become more frequent and more extended so that the limited box size can have an impact on the dynamics of the system, which is different from the quenched case. On the other hand, the change of behavior was quite abrupt and resembled similar observations made in the staggered formulation of full QCD. Here, lowering the quark mass while holding β and the (asymmetric) lattice size fixed results in a drop of the quark condensate as expected from a chiral transition and also in a rise of the Polyakov loop expectation value.

In this work we want to investigate the approach to the chiral limit somewhat further. At fixed $\beta=5.4$ we simulate two flavors of Wilson fermions by means of a hybrid Monte Carlo algorithm. On lattices of size 6^4, 9^4, and 12^4, we search for the occurrence of finite size effects when the quark mass is lowered. On the smaller lattices

we can confirm the above-mentioned observations of abrupt changes in observables like the average plaquette, the fermion condensate, and the number of conjugate gradient iterations necessary to achieve a certain accuracy in inverting the Dirac matrix. These phenomena occur at larger κ when the lattice size is increased and seem to vanish at our largest lattice, indicating that the chiral limit can be taken on large enough lattices. However, the features of the supposedly finite size effects seem interesting enough to look somewhat deeper into their origin. For that purpose, we compute quantities which are sensitive to a chiral or a finite temperature transition. In particular, we follow the evolution of the eigenvalue spectrum which is within reach of our computational capacities for the smallest lattice. We then confront the results from symmetric lattices with those obtained on an asymmetric $9^3\times 6$ lattice where the interpretation of a finite extent in the temporal direction as a finite temperature is theoretically cleaner.

Common numerical algorithms for the inclusion of dynamical fermions need vast computer resources as they require the repeated evaluation of the quark propagator throughout the equilibration process. So far most of the recent investigations of QCD with the hybrid Monte Carlo algorithm (HMCA) [3,4] have made use of the staggered fermion [5] formalism. Simulations with Wilson fermions (which have four times as many degrees of freedom) are becoming feasible only with the advent of powerful parallel machines [6,7]. This situation provides sufficient motivation to search for faster numerical methods. Intuitively, the strategy of *thinning out* the fermionic degrees of freedom could provide such a method. This approach, in which the gauge matrices are on the links of a fine lattice and the quark fields are on the sites of an associated coarse lattice, was suggested some time ago by Wilczek [8].

Within the framework of the quenched approximation, a program in this direction had been launched in form of a "renormalization-group improved" blocked Wilson fermion action[9]. It was quite successfully applied to the computation of the hadron spectrum [10] and of various hadronic matrix elements [11]. These quenched calculations allowed the pushing of lattice computations somewhat deeper into the chiral regime of small quark masses without exhausting the computational capacities available in those days.

Here, the blocking idea will be incorporated into the HMCA machinery such that the evolution of the gauge fields on the fine hypercubic lattice is driven by the usual gluonic plaquette interaction on the fine lattice and the blocked fermionic force. We apply a specific blocking procedure, "scale $\sqrt{3}$ blocking" (SQ3), whose geometry was explained in Ref. [12] and applied in detail to the fermion action in Ref. [9]. One benefit from fermion blocking is a factor 4 gain in computer requirements over the standard Wilson fermion case.

Of course, one may ask whether the use of a different lattice fermion action causes differences in the proximity to continuum physics. As a byproduct of our investigation of the chiral limit, the eigenvalue spectrum of the blocked fermion matrix shows a very close similarity with the distribution obtained from the standard Wilson form. We therefore do not expect striking differences in the approach to chiral limit between the two lattice formulations. Moreover, we computed Wilson loops in order to obtain an estimate for the string tension. The results indicate that, concerning the physical value for the lattice spacing and thus the physical lattice extent, blocked and standard Wilson formulations are in the same regime.

This paper is organized as follows. In Sec. II, we describe how fermion blocking will be technically incorporated into the dynamics of the hybrid Monte Carlo scheme. We propose to estimate the value of κ_c from the convergence rate of the standard conjugate gradient, as will be explained in Sec. III. There we also discuss some implications of the order parameters $\langle\bar{\Psi}\Psi\rangle$ and $\langle\bar{\Psi}\gamma^5\Psi\rangle$ for Wilson-like fermions. In Sec. IV, we present our numerical results, and in Sec. V we draw conclusions.

II. HYBRID MONTE CARLO AND BLOCKED FERMIONS

The usual way to discretize QCD is to put the quarks on the sites of a hypercubic lattice and the gauge fields on the respective links. The effect of the fermionic degrees of freedom on the gluonic fields is borne out off the fermion determinant $\det M$ that appears in the partition function Z of the problem. The impact of the determinant is then estimated by means of pseudofermions:

$$Z=\int\prod_{x^{(0)}\mu=1}^{4}dU_\mu(x^{(0)})\det M e^{-S_g}$$

$$=\int\prod_{x^{(0)}\mu=1}^{4}dU_\mu(x^{(0)})\prod_{x^{(0)}}d\Phi_{x^{(0)}}d\Phi^*_{x^{(0)}}e^{-(S_g+S_{\rm pf})}, \qquad (1)$$

$$S_{\rm pf}=\sum_{x^{(0)},y^{(0)}}\Phi^*_{x^{(0)}}(M)^{-1}_{x^{(0)},y^{(0)}}\Phi_{y^{(0)}},$$

where $S_{\rm pf}$ contains the inverse of the fermion matrix.

Now the main reasoning behind our way of thinning fermionic degrees of freedom goes like this: in the molecular-dynamics evolution of the gauge links, the fermionic force is dominated by the fluctuations (from configuration to configuration) among the small eigenvalues of the Dirac operator M, i.e., long-range contributions. These are expected to be preserved under the SQ3 blocking scheme, which therefore should be able to bring out the physics of the fermionic force, as it acts on the gauge fields on a fine hypercubic lattice (FHL). We emphasize that no blocking is applied to the latter.

We are thus dealing with the partition function[1]

$$Z=\int\prod_{x^{(0)}\mu=1}^{4}dU_\mu(x^{(0)})$$

$$\times\prod_{x^{(1)}}d\Phi_{x^{(1)}}d\Phi^*_{x^{(1)}}e^{-(S_g+S_{\rm blocked})}, \qquad (2)$$

[1]We have followed the usual procedure to replace $\tilde{M}$ by $\tilde{M}^\dagger\tilde{M}$ in order to assure positive definiteness of the fermion matrix. Therefore, we deal with two flavors of fermions.

where

$$S_{\text{blocked}} = \sum_{x^{(1)},y^{(1)}} \Phi^*_{x^{(1)}} (\tilde{M}^\dagger \tilde{M})^{-1}_{x^{(1)},y^{(1)}} \Phi_{y^{(1)}} .$$

The sites of the fine hypercubic lattice are denoted by $x^{(0)}$, μ enumerates the four Euclidean links (in a positive direction), with the corresponding link vectors $e^{(0)}_\mu$. The gauge field $U_\mu(x^{(0)})$ is located on the link connecting the sites $x^{(0)}$ and $x^{(0)}+e^{(0)}_\mu$, as usual. For shortness we suppress both color and Dirac indices. The pseudofermion fields $\Phi_{x^{(1)}}$ relate to the sites of the once blocked lattice (OBL), which we denote throughout this paper with the upper index (1) (1 stands for "one blocking step").

The blocked fermion matrix $\tilde{M}$ that appears in Eq. (2) has a similar, though slightly more complicated, structure as the standard Wilson action:

$$\tilde{M} = 1 - \kappa (D^{\text{diagonal}} + D^{\text{straight}}) . \tag{3}$$

Both contributions are Wilson-like hopping terms: D^{straight} connects a given block site to those neighbors on the OBL which are displaced by three links in the straight lattice directions of the FHL, while D^{diagonal} refers to an additional interaction on the OBL with certain three-link displacements on the FHL (in three dimensions, i.e., "diagonal") to be specified. They have the form [cf., Eq. (A3)]

$$\begin{aligned} D^{\text{diagonal}}_{x^{(1)},y^{(1)}} = \sum_{i=1}^{4} [& (A_1 - A_2 \gamma_i^{(1)}) \tilde{U}_i(x^{(1)}) \delta_{x^{(1)},y^{(1)}-e_i^{(1)}} \\ & + (A_1 + A_2 \gamma_i^{(1)}) \tilde{U}_i^\dagger (x^{(1)} - e_i^{(1)}) \\ & \times \delta_{x^{(1)},y^{(1)}+e_i^{(1)}}] , \\ D^{\text{straight}}_{x^{(1)},y^{(1)}} = \sum_{i=5}^{8} [& (A_3 - A_4 \gamma_i^{(1)}) \tilde{U}_i(x^{(1)}) \delta_{x^{(1)},y^{(1)}-e_i^{(1)}} \\ & + (A_3 + A_4 \gamma_i^{(1)}) \tilde{U}_i^\dagger (x^{(1)} - e_i^{(1)}) \\ & \times \delta_{x^{(1)},y^{(1)}+e_i^{(1)}}] . \end{aligned} \tag{4}$$

Our geometric nomenclature[2] closely follows Ref. [9]: $e_i^{(1)}$ is the direction vector in the ith direction; note that i now ranges from 1 to 8, as the blocking of the fermion matrix M creates the additional nearest-neighbor interactions in four diagonal directions. The A_j's are blocking constants. The $\gamma_i^{(1)}$'s are constructed from the usual Dirac matrices. The effective links $\tilde{U}_i(x^{(1)})$ are related to the OBL links and appear exclusively in the blocked fermionic action and the fermionic force.[3]

To carry through molecular dynamics, we follow Refs. [3,4] and add momenta $P_{x^{(0)},\mu}$, conjugate to the gauge fields, i.e., located on the FHL. The resulting Hamiltonian reads

$$\begin{aligned} H = & \tfrac{1}{2} \sum_{x^{(0)},\mu} \text{tr} P^2_{x^{(0)},\mu} + \beta \sum_{x^{(0)},\mu\nu>\mu} \sum [1 - \tfrac{1}{6} \text{tr}(U_{\mu\nu} + \text{H.c.})] \\ & + \sum_{x^{(1)},y^{(1)}} \Phi^*_{x^{(1)}} (\tilde{M}^\dagger \tilde{M})^{-1}_{x^{(1)},y^{(1)}} \Phi_{y^{(1)}} . \end{aligned} \tag{5}$$

In order to construct the equation of motion for $P_{x^{(0)},\mu}$ with respect to τ, one still can apply the idea of Ref. [4]. Start from the conservation of H, i.e., $\dot{H}=0$. For the fermionic part of the problem, this now involves the computation of the time derivative of the effective links $\tilde{U}_i(x^{(1)})$. Since $\tilde{U}_i(x^{(1)})$ is a sum of products of three links on the FHL [cf., Eq. (A4)], $\dot{\tilde{U}}_i(x^{(1)})$ can again be expressed in terms of $U_\mu(x^{(0)})$. Isolating $\dot{P}_{x^{(0)},\mu}$ on the left-hand side,

$$i\dot{P}_{x^{(0)},\mu} = U_\mu(x^{(0)}) \left\{ \left[-\frac{\beta}{6} V_{x^{(0)},\mu} + F_{x^{(0)},\mu}[U_\mu(x^{(0)})] \right] - \text{H.c.} \right\} , \tag{6}$$

we find the starting point for the molecular-dynamics procedure with a blocked fermion force. The curly brackets contain the standard sum over staples $V_{x^{(0)},\mu}$ attached to the gauge link $U_\mu(x^{(0)})$, and the fermionic contribution $F_{x^{(0)},\mu}$, the explicit form of which can be found in Eq. (A8) and Table III. Now HMC blocking (HMCB) proceeds: Calculate the evolution of the gauge links on the FHL in phase space with blocked fermionic force; carry out the Metropolis decision, taking into account the gauge action and conjugate momenta on the FHL and the fermionic action on the OBL.

In the numerical implementation of HMCB, we applied the well-established standard conjugate gradient algorithm to the inversion of the blocked fermionic matrix in view of its advantageous limitation in the number of control parameters. As residue (norm of the residual vector) we used $R = 10^{-4}$. All calculations presented here were performed at $\beta = 5.4$. We performed 20 molecular-dynamics steps between each Metropolis decision and gained acceptance rates of about 75% with a time step size ϵ of 0.04 on a 6^4 lattice for all κ values used. On the 12^4 lattice, we had to reduce ϵ to the value 0.015 in order to assure the same acceptance rate.

TABLE I. Direction vectors of a FHL and a OBL in units of the FHL spacing. $\bar{1}$ stands for -1.

FHL	OBL	
$e_1^{(0)}=(1,0,0,0)$	$e_1^{(1)}=(1,1,1,0)$	$e_5^{(1)}=(3,0,0,0)$
$e_2^{(0)}=(0,1,0,0)$	$e_2^{(1)}=(\bar{1},1,0,1)$	$e_6^{(1)}=(0,3,0,0)$
$e_3^{(0)}=(0,0,1,0)$	$e_3^{(1)}=(1,0,\bar{1},1)$	$e_7^{(1)}=(0,0,3,0)$
$e_4^{(0)}=(0,0,0,1)$	$e_4^{(1)}=(0,\bar{1},1,1)$	$e_8^{(1)}=(0,0,0,3)$

[2]To make the paper self-contained, we give a review of the geometry of SQ3 and of the blocking procedure in the Appendix.

[3]Note that, for periodic closure, one is restricted to lattice sizes which are integer multiples of 3.

III. TOOLS TO STUDY DECONFINEMENT AND CHIRAL TRANSITIONS

We monitored the approach to the chiral limit by measuring observables which promise to give insight into the nature of a transition phenomenon which, in the following, we would like to call "shielding" before another interpretation can be given. In the pure gauge theory, the Polyakov loop P is the order parameter which signals the deconfinement phase transition at finite temperature. In that theory the behavior of the Polyakov loop on a finite lattice reflects the spontaneous breaking of the Z_3 symmetry of its action. When quark loops are included in the action, the interpretation of the Polyakov loop becomes subtle. Because of fermionic contribution, the Z_3 symmetry of the action is explicitly broken; yet numerical calculations based on the staggered quark formalism still show a sharp transition [5] which manifests itself through a sharp rise in the vacuum expectation value of the Polyakov loop P.

At this transition, normally referred to as the finite temperature deconfinement transition, $\langle\bar{\Psi}\Psi\rangle$ for the staggered fermions is observed to drop to zero in the limit of vanishing quark mass, indicating the restoration of chiral symmetry [5]. This is not at all obvious with Wilson fermions due to the Wilson term. Nevertheless, we also measure the unrenormalized chiral condensate. This observable is strongly dependent on the small eigenvalues of the hopping term D in the fermion matrix M, $M=1-\kappa D$. Since these eigenvalues are controlled by closed quark loops it is reasonable to expect that, at light quark mass, the behavior of this observable is strongly correlated to that of the expectation value of the Polyakov loop. Hence, it should be strongly affected if the shielding has the signature of a finite temperature transition.

The chiral condensate can be cast into the form of a spectral representation

$$\langle\bar{\Psi}\Psi\rangle=\frac{1}{V}\sum_i\frac{1}{1-\kappa\lambda_i}\ , \tag{7}$$

where λ_i are the eigenvalues of D and V is the lattice volume. The "γ^5 symmetry" of D, $\gamma^5 D\gamma^5=D^\dagger$, requires that the complex eigenvalues of D appear in complex conjugate pairs λ and λ^*. Hence, the condensate is real on each configuration.

From the above representation, Eq. (7), it is obvious that a real eigenvalue of D, λ_r, would give rise to a pole in the condensate $\langle\bar{\Psi}\Psi\rangle$ at the appropriate value of the hopping parameter, $\kappa=1/\lambda_r$; vice versa, if a sudden drop in $\langle\bar{\Psi}\Psi\rangle$ signals a chiral phase trasnition, one would expect a corresponding abrupt change in the eigenvalue distribution of D. In particular, one would expect any previously real eigenvalues to move into the complex plane.

A third observable is $\langle\bar{\Psi}\gamma^5\Psi\rangle$ which can be regarded as the order parameter for parity violation [13]. This order parameter also depends strongly on the distribution of the eigenvalues of D, but, in addition, it has a strong dependence on the behavior of their associated eigenvectors. If R_i denotes an eigenvector of D with eigenvalue λ_i, i.e., $DR_i=\lambda_i R_i$, and $\tilde{R}_i$ is the corresponding eigenvector for λ_i^* normalized such that $\tilde{R}_i^\dagger\gamma_5 R_j=\delta_{ij}$, then $\langle\bar{\Psi}\gamma^5\Psi\rangle$ can be written as

$$\langle\bar{\Psi}\gamma^5\Psi\rangle=\frac{1}{V}\sum_i\frac{\tilde{R}_i^\dagger R_i}{1-\kappa\lambda_i}\ . \tag{8}$$

Again, we see that the distribution of eigenvalues close to $1/\kappa$ will strongly influence the behavior of this observable which is real on each configuration as well.

We use the Lanczos algorithm to tridiagonalize the hopping term [14] and then the quenched lattice (QL) algorithm with implicit shifts to obtain the eigenvalues. However, the structure of the Wilson matrix arising from the fermionic action is such that, at present, it is not possible to compute all its eigenvalues unless orthogonality is maintained between the Lanczos vectors developed in the algorithm. Since this requires all these vectors to be stored, the available computer memory limits the maximum lattice size to 4^4 upon which the spectral properities of Wilson fermions can be studied. However, because of the SQ3 blocking and the ensuing reduction of the fermionic degrees of freedom on the once blocked lattice, we can study the eigenvalue distributions on a 6^4 lattice. Since we have to know, and store, all the Lanczos vectors, it is straightforward to extend the QL algorithm to obtain the above eigenvectors. Note that the measurement of $\langle\bar{\Psi}\gamma^5\Psi\rangle$ could also be obtained directly from the eigenvalues of $\gamma_5 M$ without the requirement of reorthogonalization since it is Hermitian.

We have two ways of computing $\langle\bar{\Psi}\Psi\rangle$: we can use the spectral representation, Eq. (7), or we can apply (and in this way check) the stochastic estimator (SE) method [15] which is based on the computation of the quark propagator from a stochastic extended source (instead of a point source). We also perform a stochastic estimate of $\langle(\bar{\Psi}\gamma^5\Psi)^2\rangle_0$ as monitor; here $\langle\ \rangle_0$ stands for the joint average over gauge fields and stochastic estimator sources.[4]

Strictly speaking, a precise determination of κ_c on small lattices is excluded because of the prior appearance of the shielding: normal methods, such as those described above, fail in the region $\kappa>\kappa_s$. Thus, we have to provide ourselves with some suitable control parameter from which we can estimate, by extrapolation through κ_s, the chiral limit. We show below that the convergence rate of the conjugate gradient algorithm might act as such a parameter.

In order to do this, we start from the definition of κ_c as the value of the hopping parameter κ at which the pion mass vanishes [resulting from renormalized Ward identi-

[4]The observable $\langle(\bar{\Psi}\gamma^5\Psi)^2\rangle_0$ is closely related to the "pion norm" introduced in Ref. [2]. There the pion norm is used to monitor the region of "criticality." As one moves the hopping parameter κ closer to κ_c, one expects the system to become critical more frequently; i.e., one can observe an increasing number of sharp peaks in the time evolution of the pion norm. However, we could merely get a rough idea of the location of κ_c by using this method.

ty and PCAC (partial conservation of axial-vector current) relations [16–18]],

$$m_\pi^2 \propto m_q = \frac{1}{2}\left[\frac{1}{\kappa} - \frac{1}{\kappa_c}\right] . \tag{9}$$

In addition, there is a theorem concerning the convergence rate of the conjugate gradient algorithm: for a number of N_{CG} iteration steps, the norm of the residual vector R is bound by [19]

$$R \leq 2\left[\frac{\sqrt{\lambda_{\max}} - \sqrt{\lambda_{\min}}}{\sqrt{\lambda_{\max}} + \sqrt{\lambda_{\min}}}\right]^{N_{\mathrm{CG}}} . \tag{10}$$

This result is certainly valid for a uniform distribution of eigenvalues. There will be some dependence of R on the detailed distribution of eigenvalues, in particular around $\lambda_{\min}$ where the dependence on the spectral density could be critical in controlling the conjugate gradient convergence. However, it does provide a first-order approximation to the convergence behavior of $M^\dagger M$. We shall show below that, prior to the shielding, it is completely consistent with the observed convergence of the algorithm.

Close to κ_c the minimal real eigenvalue of $M^\dagger M$ is small and is approximately that of M^2, i.e., $(1-\kappa/\kappa_c)^2$. It follows from the above that, for the inversion of $M^\dagger M$, the number of iterations required for convergence of the algorithm to some small but fixed residual R will behave as

$$\frac{1}{N_{\mathrm{CG}}} \propto 2\kappa m_q = \frac{\kappa_c - \kappa}{\kappa_c} . \tag{11}$$

We shall subsequently verify the validity of this equation prior to the shielding and use it to perform a linear extrapolation to the true chiral limit.

IV. RESULTS

In order to study the approach to the chiral limit with Wilson fermions, we performed simulations on symmetric lattices of increasing size 6^4, 9^4, and 12^4. The coupling was fixed to $\beta=5.4$. In the first round of exploration we measured the gauge field action and the (unsubtracted) chiral condensate $\langle\bar{\Psi}\Psi\rangle$ working at equal values of the valence and the dynamic hopping parameters, $\kappa^{(\mathrm{val})}=\kappa$. As discussed in Sec. III, we attempted to use the number of conjugate gradient iterations necessary to achieve a certain accuracy for the inverse Dirac matrix as a cheap means to extrapolate to the chiral limit. These inversions are needed for the calculation of the fermionic force in the molecular-dynamics steps anyway and no further inversions for, e.g., computing the pion propagator are required. We found that, at an accuracy of 10^{-4} for the conjugate gradient residue, N_{CG} varies only very little over the simulated trajectories. In Fig. 1, we show our results for these three quantities on the 6^4 lattice. We observe a sudden decrease in the gauge field action and the chiral condensate when κ is increased. This is accompanied by an apparently correlated rise in $1/N_{\mathrm{CG}}$ (let us call this point κ_s, where s stands for shielding). As depicted in Fig. 2, the κ value where $1/N_{\mathrm{CG}}$ develops a minimum depends on the lattice size and shifts to larger values of κ when the lattice is enlarged. On the 12^4 lattice, $1/N_{\mathrm{CG}}$ deviates only weakly from a linear behavior.

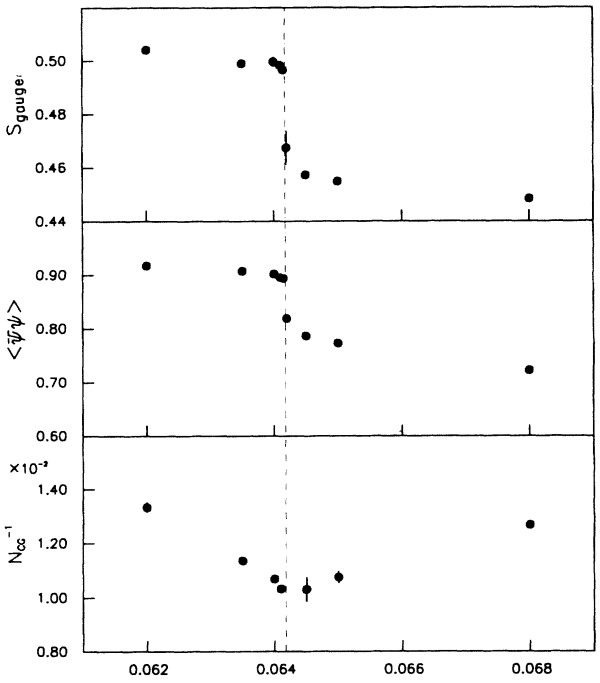

FIG. 1. S_{gauge}, $\langle\bar{\Psi}\Psi\rangle$, $\langle(\bar{\Psi}\gamma^5\Psi)^2\rangle_0$, and $1/N_{\mathrm{CG}}$ vs κ at $\beta=5.4$ on a 6^4 lattice.

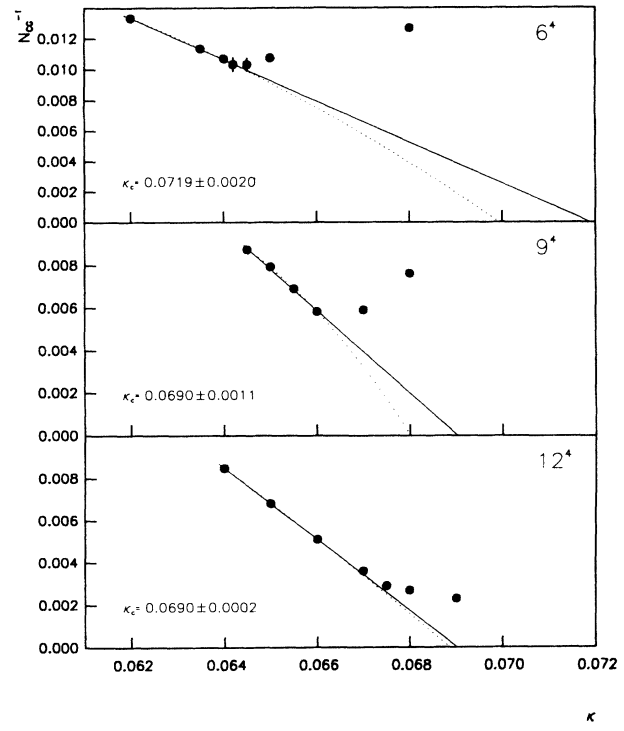

FIG. 2. Extrapolation to κ_c for the symmetric 6^4, 9^4, and 12^4 lattices.

We take this as evidence that these effects are due to the finite size of the lattice and disappear at our value of β on a 12^4 lattice. Thus, on sufficiently large lattices it seems to be possible to obtain the chiral limit in the standard way. Prior to the sudden change in behavior, $1/N_{CG}$ shows quite a linear dependence on κ lending support to the applicability of Eq. (11). When we extrapolate to the value of κ where N_{CG} becomes infinite, we obtain a value of $\kappa_c = 0.069$ almost independent of the lattice size. On an infinite lattice this point supposedly corresponds to a zero mode in the fermion matrix and would be the location where the chiral limit has to be taken.

It is obviously of interest to study the nature of these finite size effects in somewhat more detail. We have therefore followed two lines which have been within our computational capabilities: on a 6^4 lattice we have performed a more detailed study including a computation of the eigenvalue spectrum of the fermion matrix. Second, we carried out an investigation on an asymmetric lattice of size $9^3 \times 6$ where finite size effects may be mainly due to the small temporal extent and thus be finite temperature physics.

For the 6^4 lattice, in Fig. 3 we present our results for the gauge action $\langle \bar{\Psi}\Psi \rangle$, $\langle (\bar{\Psi}\gamma^5\Psi)^2 \rangle_0$, and also $\langle \bar{\Psi}\gamma^5\Psi \rangle$. There is an abrupt change in all four quantities at the same κ value denoted κ_s. In Fig. 4 we display the behavior of the Polyakov loop distribution as κ moves through this shielding point κ_s. We observe a sudden change in the scatterplot from a spherical to a *Mercedes*-star shape. Note that there is some tunneling into all three vacua even beyond the shielding point. In contrast with the results of Bitar *et al.*, who found Im(P) to be negligibly small in both phases, we do observe genuine complex behavior with a definite three-vacua structure in the "deconfined" phase.

The 6^4 lattice is small enough to allow the determination of the full eigenvalue spectrum (and the associated eigenvectors) using the Lanczos method outlined above as applied to the once blocked hopping matrix D. Typical spectra for a configuration at a given κ are shown in Fig. 5. They are very similar in shape and structure to those obtained in a quenched standard Wilson simulation in SU(2) on a 4^4 lattice [20], where there is an elliptical "hamburger" shape with cavities developing as the finite temperature transition is approached.

We have used the eigenvalues to calculate $\langle \bar{\Psi}\Psi \rangle$ via Eq. (7) and, in conjunction with their eigenvectors, to calculate $\langle \bar{\Psi}\gamma^5\Psi \rangle$ via Eq. (8). In Fig. 3, we compare $\langle \bar{\Psi}\Psi \rangle$ calculated from the spectrum with $\langle \bar{\Psi}\Psi \rangle$ as obtained by means of the SE method and find good agreement. The respective contributions to $\langle \bar{\Psi}\gamma^5\Psi \rangle$ of the purely real eigenvalues and of the eigenvalues with a nonvanishing imaginary part are shown in the fourth window of Fig. 3. Both contributions cancel each other largely. We thus have no evidence for parity violation on either side of the shielding point.

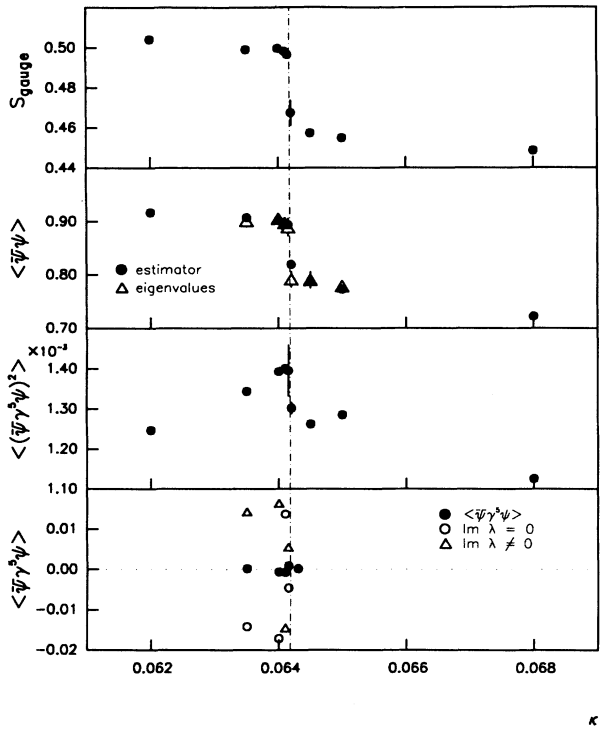

FIG. 3. S_{gauge}, $\langle \bar{\Psi}\Psi \rangle$, $\langle (\bar{\Psi}\gamma^5\Psi)^2 \rangle_0$, and $\langle \bar{\Psi}\gamma^5\Psi \rangle$ vs κ at $\beta = 5.4$ on a 6^4 lattice. $\langle \bar{\Psi}\Psi \rangle$ has been calculated by the stochastic estimator method and also via the eigenvalues. The respective contributions of real and complex eigenvalues to $\langle \bar{\Psi}\gamma^5\Psi \rangle$ cancel largely on both sides of the phase transition.

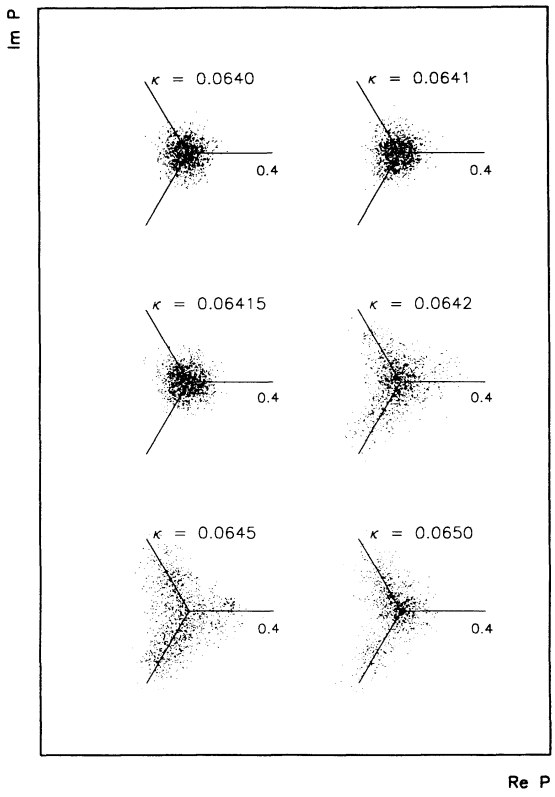

FIG. 4. The Polyakov loop distribution on a 6^4 lattice. The spherical distribution converts to a *Mercedes*-star-like shape, reflecting the tunneling into the three possible vacua.

Each of the eigenvalue distributions shown in Fig. 5 is actually a snapshot at a given moment in molecular-dynamics time. Generally speaking, they change from a fairly uniform and nearly spherical structure at low κ through elliptical "hamburgerlike" shapes into a distribution where real eigenvalues are increasingly thinned out. This sequence of shapes is characteristic as a function of κ. Following the time history of the system at a given κ, just above κ_s one actually observes a flip-flop behavior of a series of distributions with real eigenvalues followed (in molecular-dynamics time) by a series with no real eigenvalues as demonstrated in Fig. 6. Corresponding to the density of real eigenvalues, $\langle\bar{\Psi}\Psi\rangle$ decreases. At $\kappa=0.0645$ the surviving real eigenvalues cluster around the corresponding locations of the free theory. At larger κ values, the distribution develops a gap along the real axis. In these respects this behavior prior to, at, and beyond the shielding point is similar to that observed in quenched simulations around the finite temperature phase transition [20].

We now discuss our results on an asymmetric $9^3\times6$ lattice. In Fig. 7, we show the gauge field action $\langle\bar{\Psi}\Psi\rangle$ and $\langle(\bar{\Psi}\gamma^5\Psi)^2\rangle_0$ as a function of the hopping parameter. Again, with increasing κ, the values of S_{gauge} and the quark condensate decrease in an apparently correlated

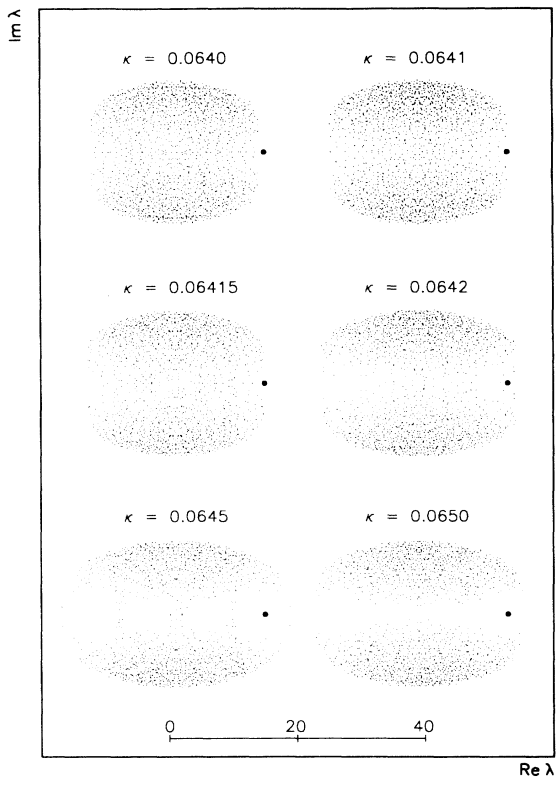

FIG. 5. Change in the eigenvalue distribution across the phase transition. Each picture is a typical representant borrowed from a series of configurations at equal κ. The bold point denotes the location of κ_c as obtained by extrapolation of $1/N_{\text{CG}}$ (Fig. 2). The scale drawn in is valid for both the abscissa and the ordinate.

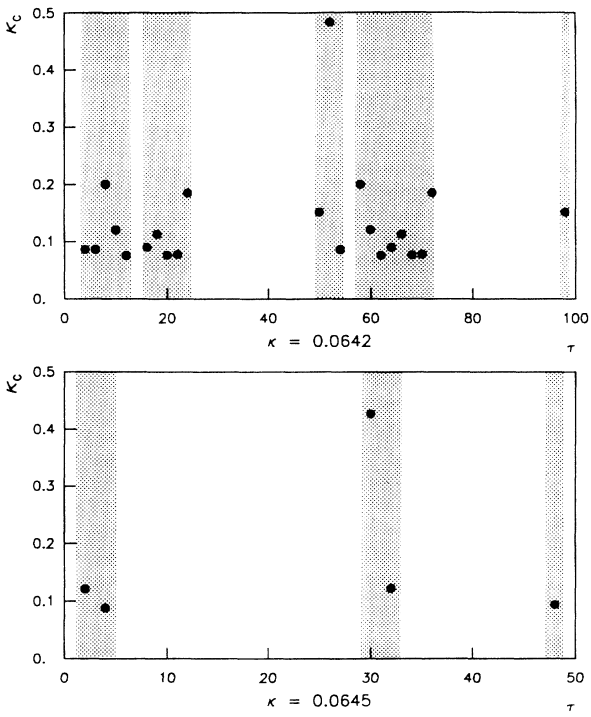

FIG. 6. Flip-flop behavior for $\kappa>\kappa_s$ on a 6^4 lattice. $1/\lambda^r_{\text{max}}$ is plotted as function of the molecular-dynamics time τ for two values of κ. The shadows denote the regions where purely real eigenvalues of the fermion matrix occur.

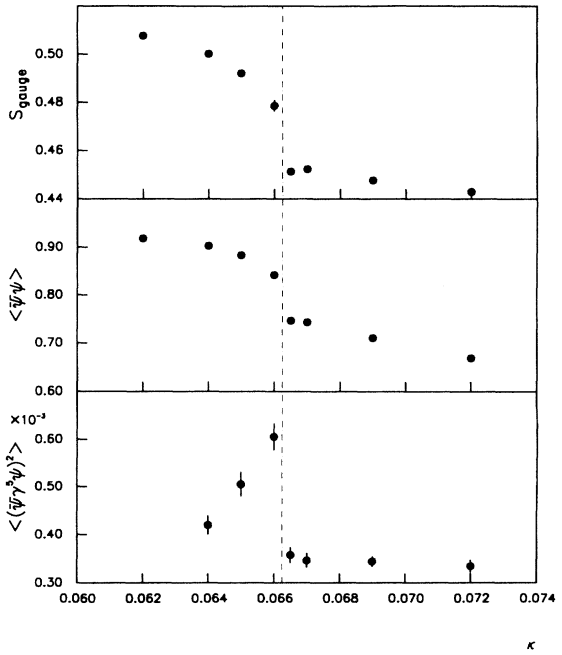

FIG. 7. S_{gauge}, $\langle\bar{\Psi}\Psi\rangle$, and $\langle(\bar{\Psi}\gamma^5\Psi)^2\rangle_0$ vs κ at $\beta=5.4$ on a $9^3\times6$ lattice. The vertical line shows the location of the shielding transition.

manner. Both observables drop suddenly at the same value of $\kappa=\kappa_s\approx 0.0662$. On the other hand, $\langle(\bar{\Psi}\gamma^5\Psi)^2\rangle_0$ rises as κ approaches κ_s from below, but it also exhibits a jump at the same κ. Likewise, Fig. 8 shows the inverse of the number of conjugate gradient iteration steps, $1/N_{\rm CG}$ (necessary to achieve the conjugate gradient residue $R=10^{-4}$), as a function of the hopping parameter κ. As on the symmetric lattices, there is a definite linear behavior of $1/N_{\rm CG}$ in κ prior to κ_s. A straight-line extrapolation to the limit $N_{\rm CG}=\infty$ gives $\kappa_c=0.0676\pm 0.0003$, significantly above $\kappa_s=0.0662$. The error quoted for κ_c is estimated from an alternative quadratic fit. This point agrees precisely with the location where the Polyakov loop undergoes a sudden change in behavior as well, as shown in Fig. 9: the scatterplot of P looses isotropy and chooses a preferred orientation along one of the Z_3 vacua. All these phenomena resemble very closely the features observed in the vicinity of the deconfinement transition in quenched calculations [22].

Beyond the shielding point, the behavior of $1/N_{\rm CG}$ and $\langle(\bar{\Psi}\gamma^5\Psi)^2\rangle_0$ hints at an increase of the pion mass and can be compared with the features first found by DeTar and Kogut [21] in the staggered fermion formalism. There a rise in the pion mass between the confined phase and the quark-gluon plasma could be attributed to the restoration of chiral symmetry.

Since we have used fermionic degrees of freedom thinned out by applying a SQ3 blocking to the standard Wilson action, one might ask whether a simulation with the blocked action is similarly close to continuum physics (on the same lattice) as the conventional approach with standard Wilson fermions. A precise answer would require a mapping of the parameters κ and β on unblocked

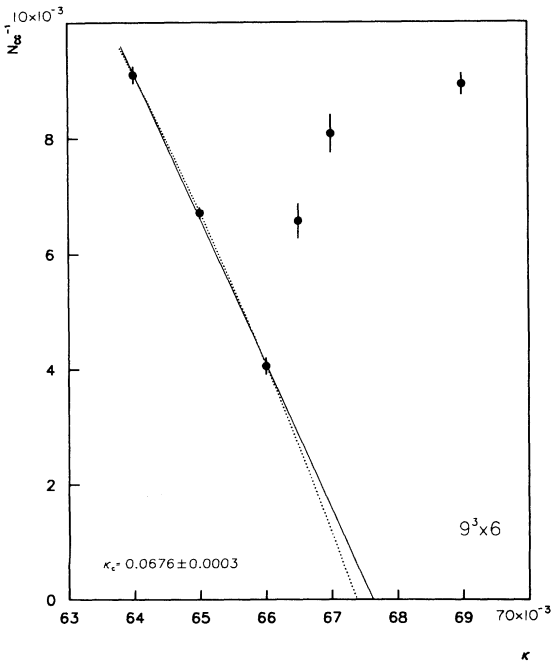

FIG. 8. Extrapolation to κ_c for the $9^3\times 6$ lattice (the solid line is a linear fit). The error follows from the polynomial fit (dashed line).

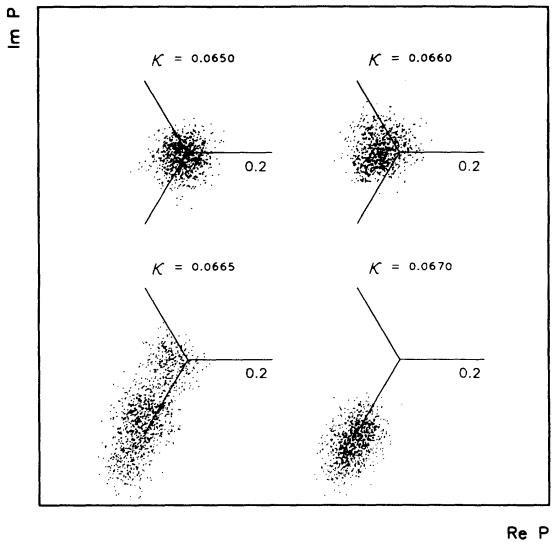

FIG. 9. The Polyakov loop distribution for various κ values at $\beta=5.4$ for the $9^3\times 6$ lattice.

κ and β values. Within the context of this exploratory work, we have restricted ourselves to measure Creutz ratios on the 9^4 lattice at $\kappa=0.064$ in order to estimate the length scale in our simulation. We find that the lattice spacing (deduced from the string tension) with blocked dynamical fermions appears to be about the same size as that of standard dynamical Wilson [23] fermions at equal β. This is good news since we apparently do not step away from continuum physics by blocking fermionic degrees of freedom.

V. SUMMARY AND CONCLUSIONS

By blocking fermionic degrees of freedom, we extended previous full QCD studies on the approach to the chiral limit. This blocking procedure enabled us to study the evolution of the eigenvalue spectrum $\{\lambda\}$ of the fermionic matrix through the shielding point on a 6^4 lattice. The behavior of these distribution, considered as a function of κ, is very similar to that observed in the β dependence of the quenched theory around its deconfinement transition; i.e., the passing through the shielding point is accompanied by the appearance of a gap in the eigenvalue distribution along the real axis in the complex λ plane. In many respects the qualitative behavior of the spectral distribution appears to be consistent with that through a chiral transition. It would be very interesting to extend such studies on topological features of the action [24].

The performance of the conjugate gradient iteration scheme is strongly dependent upon the lower spectral bound. The convergence rate allowed us to study the limiting behavior on lattices up to 12^4 in detail and, moreover, to estimate how close we are to the chiral limit. The location of the chiral limit determined in this way is approached by the shielding point with growing lattice size, the latter being reasonably close to κ_c at $\beta=5.4$ on the 12^4 lattice. This indicates that, on symmetric lattices,

shielding disappears when the lattice is large enough and thus is a finite size effect.

On the asymmetric lattice, the same effects occur and are even more pronounced. We certainly cannot claim to observe genuine finite temperature physics, given the spatial size of 9^3 compared to $N_\tau=6$. Nevertheless, taken as a whole, our results seem to suggest a deconfinement and/or chiral transition mechanism as the origin of the observed finite size effects. If so, then the abrupt changes in the observables P, $\langle\bar{\Psi}\Psi\rangle$, and $\langle(\bar{\Psi}\gamma^5\Psi)^2\rangle_0$, together with the observed flipflop behavior of the spectral distribution at the transition point κ_s, would hint at a first- rather than a second-order phase transition.

Clearly, in order to reach conclusive answers as to the nature of the transition, much more computational effort would be needed.

ACKNOWLEDGMENTS

We are grateful to Rainer Sommer for discussions and useful hints. I. B. would like to thank Fritz Gutbrod and his colleagues at HLRZ, where this work was initiated, for their kind hospitality. The computations were performed on the SIEMENS VP400-EX Supercomputer at the Rechenzentrum of the University of Karlsruhe. We are thankful to the staff of the computer center for their kind support. This work was supported in part by Deutsche Forschungsgemeinschaft Grant No. Schi 257/1-2.

APPENDIX

In the following we explicate the geometry of the OBL and the blocking scheme which leads to the blocked fermion matrix. Subsequently, we present in detail the blocked fermionic force in terms of the gauge fields of a FHL. Our notation differs slightly from Ref. [9].

1. Geometry of OBL

A four-dimensional fine hypercubic lattice, the sites of which are integer multiples of 3, can be subdivided into nonoverlapping blocks. Each block contains nine sites, the central site $x^{(1)}$ belonging to the resulting once blocked lattice and its eight nearest neighbors. One block contains the sites

$$x^{(1)},\quad x^{(1)}+e_\mu^{(0)},\ \mu\in\{1,\ldots,4\},\quad x^{(1)}-e_\mu^{(0)},\ \mu\in\{1,\ldots,4\}. \tag{A1}$$

The blocking procedure of Sec. 2 will end in diagonal and straight interactions. Table I shows the direction vectors (in positive direction only) of the FHL and the OBL in lattice units of the FHL which are set equal 1. We denote the nearest neighbors by $y^{(1)}$. They are associated to $x^{(1)}$ according to

$$y^{(1)}=x^{(1)}+e_i^{(1)}=x^{(1)}+e_\rho^{(0)}+e_\mu^{(0)}+e_\sigma^{(0)},\quad i\in\{1,\ldots,8\}. \tag{A2}$$

Table I immediately shows that the nearest-neighbor sites into the four positive diagonal directions ($i\in1,\ldots,4$) can each be connected via 6 topologically equivalent shortest paths represented in Table II. There is only one possible shortest path in each of the straight directions ($i\in5,\ldots,8$). Therefore, together with the 24 diagonal paths, we get 28 shortest paths on a FHL connecting $x^{(1)}$ on a OBL with its nearest neighbors on a OBL in a positive direction. Each path has been given a definite number. Figure 10 shows two paths, one going in a straight direction, denoted by the direction vector $e_5^{(1)}$ and the other going in diagonal direction, which is given by the direction vector $e_1^{(1)}$ of Table I. Only one of the six topologically equivalent paths is drawn.

TABLE II. 4×6 topologically equivalent diagonal and four straight paths on a FHL connecting nearest neighbors in positive diagonal directions.

	$e_1^{(1)}$				$e_2^{(1)}$				$e_3^{(1)}$				$e_4^{(1)}$			
No.	ρ	μ	σ	No.	ρ	μ	σ	No.	ρ	μ	σ	No.	ρ	μ	σ
1	1	2	3	7	$\bar{1}$	2	4	13	1	$\bar{3}$	4	19	$\bar{2}$	3	4
2	1	3	2	8	$\bar{1}$	4	2	14	1	4	$\bar{3}$	20	$\bar{2}$	4	3
3	2	1	3	9	2	$\bar{1}$	4	15	$\bar{3}$	1	4	21	3	$\bar{2}$	4
4	2	3	1	10	2	4	$\bar{1}$	16	$\bar{3}$	4	1	22	3	4	$\bar{2}$
5	3	1	2	11	4	$\bar{1}$	2	17	4	1	$\bar{3}$	23	4	$\bar{2}$	3
6	3	2	1	12	4	2	$\bar{1}$	18	4	$\bar{3}$	1	24	4	3	$\bar{2}$
	$e_5^{(1)}$				$e_6^{(1)}$				$e_7^{(1)}$				$e_8^{(1)}$			
No.	ρ	μ	σ	No.	ρ	μ	σ	No.	ρ	μ	σ	No.	ρ	μ	σ
25	1	1	1	26	2	2	2	27	3	3	3	28	4	4	4

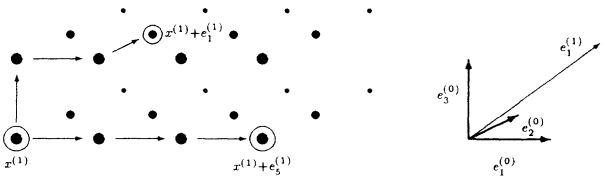

FIG. 10. Hyperplane of a FHL. A circle around a disk denotes a site of a OBL.

2. Blocking procedure

The SQ3 blocking can be described schematically in three steps.

(1) Express the Wilson action on a FHL in terms of the coordinates $x^{(1)}$ and 9 internal degrees of freedom μ of a OBL, $\mu\in\{-4,\ldots,0,\ldots,4\}$.

(2) Diagonalize the mass terms of the reformulated Wilson action with respect to the space of the internal degrees of freedom and separate the fermionic determinant according to light and heavy modes; the latter can be integrated out taking away the 8 heavy modes (8 degrees of freedom).

(3) Truncate the higher-order terms in an expansion of the remaining effective fermionic matrix. The infrared behavior of the theory should be unaffected.

These blocking steps are explained in detail in Ref. [9]. They result in the following blocked fermion matrix:

$$\tilde{M}_{x^{(1)},y^{(1)}}=2m\delta_{x^{(1)},y^{(1)}}-\sum_{1=1}^{4}A_1[\tilde{U}_i(x^{(1)})\delta_{x^{(1)},y^{(1)}-e_i^{(1)}}+\tilde{U}_{-i}(x^{(1)})\delta_{x^{(1)},y^{(1)}+e_i^{(1)}}-2\delta_{x^{(1)},y^{(1)}}]$$
$$-\sum_{i=5}^{8}A_3[\tilde{U}_i(x^{(1)})\delta_{x^{(1)},y^{(1)}-e_i^{(1)}}+\tilde{U}_{-i}(x^{(1)})\delta_{x^{(1)},y^{(1)}+e_i^{(1)}}-2\delta_{x^{(1)},y^{(1)}}]$$
$$-\sum_{i=1}^{4}A_2\gamma_i^{(1)}[\tilde{U}_i(x^{(1)})\delta_{x^{(1)},y^{(1)}-e_i^{(1)}}-\tilde{U}_{-i}(x^{(1)})\delta_{x^{(1)},y^{(1)}+e_i^{(1)}}]$$
$$-\sum_{i=5}^{8}A_4\gamma_i^{(1)}[\tilde{U}_i(x^{(1)})\delta_{x^{(1)},y^{(1)}-e_i^{(1)}}-\tilde{U}_{-i}(x^{(1)})\delta_{x^{(1)},y^{(1)}+e_i^{(1)}}]\ . \tag{A3}$$

The blocking introduces effective links $\tilde{U}$ which are sums of products of fine links U on a FHL:

$$\tilde{U}_i(x^{(1)})=\begin{cases}\frac{1}{6}\sum\limits_{\substack{6\text{ topol.}\\ \text{equiv.}\\ \text{paths}}}U_\rho(x^{(1)})U_\mu(x^{(0)})U_\sigma(y^{(0)}) & \text{for } i\in\{1,\ldots,4\},\\ U_\rho(x^{(1)})U_\mu(x^{(0)})U_\sigma(y^{(0)}) & \text{for } i\in\{5,\ldots,8\}.\end{cases} \tag{A4}$$

One can show (cf. Ref. [9]) that an iteration of the blocking will result in the same structure in every blocking step. The blocking parameters A_i that are actually used are $A_1=4.242$, $A_2=2.598$, $A_3=0.0976$, and $A_4=0.0481$.

The direction vectors must satisfy the conditions

$$x^{(0)}=x^{(1)}+e_\rho^{(0)},\quad y^{(0)}=x^{(0)}+e_\mu^{(0)},\quad y^{(1)}=y^{(0)}+e_\sigma^{(0)}\ ,$$
$$y^{(1)}=x^{(1)}+e_i^{(1)},\quad e_i^{(1)}=e_\rho^{(0)}+e_\mu^{(0)}+e_\sigma^{(0)}\ , \tag{A5}$$

with $\rho,\mu,\sigma\in\{-4,\ldots,4\}$. The $\gamma_i^{(1)}$'s are constructed from the FHL $\gamma_\mu^{(0)}$'s:

$$\gamma_i^{(1)}=(\gamma^{(0)},e_i^{(1)})\ . \tag{A6}$$

3. Fermionic force

The time derivative of the fermionic part of the Hamiltonian [Eq. (5)] contains a diagonal, $i=\{1,\ldots,4\}$, and a straight contribution, $i=\{5,\ldots,8\}$ (trace over color and Dirac indices assumed); it can be cast into the form

$$\frac{dS}{d\tau}=\frac{dS_d}{d\tau}+\frac{dS_s}{d\tau}=\kappa\sum_{x^{(1)}}\sum_{i=1}^{8}\{\dot{\tilde{U}}_i(x^{(1)})P_{x^{(1)},i}+\dot{\tilde{U}}_i^\dagger(x^{(1)}-e_i^{(1)})P_{x^{(1)},-i}\}\ , \tag{A7}$$

where

$$\left.\begin{aligned}P_{x^{(1)},i}&=Y_{x^{(1)}+e_i^{(1)}}X_{x^{(1)}}^\dagger(A_1+A_2\gamma_i^{(1)})+X_{x^{(1)}+e_i^{(1)}}Y_{x^{(1)}}^\dagger(A_1-A_2\gamma_i^{(1)}),\\ P_{x^{(1)},-i}&=X_{x^{(1)}-e_i^{(1)}}Y_{x^{(1)}}^\dagger(A_1+A_2\gamma_i^{(1)})+Y_{x^{(1)}-e_i^{(1)}}X_{x^{(1)}}^\dagger(A_1-A_2\gamma_i^{(1)}),\end{aligned}\right\}\ i=\{1,\ldots,4\}\ ,$$

$$\left.\begin{aligned}P_{x^{(1)},i}&=Y_{x^{(1)}+e_i^{(1)}}X_{x^{(1)}}^\dagger(A_3+A_4\gamma_i^{(1)})+X_{x^{(1)}+e_i^{(1)}}Y_{x^{(1)}}^\dagger(A_3-A_4\gamma_i^{(1)}),\\ P_{x^{(1)},-i}&=X_{x^{(1)}-e_i^{(1)}}Y_{x^{(1)}}^\dagger(A_3+A_4\gamma_i^{(1)})+Y_{x^{(1)}-e_i^{(1)}}X_{x^{(1)}}^\dagger(A_3-A_4\gamma_i^{(1)}),\end{aligned}\right\}\ i=\{5,\ldots,8\}\ ,$$

with

$$X=(\tilde{M}^\dagger\tilde{M})^{-1}\Phi,\quad Y=\tilde{M}(\tilde{M}^\dagger\tilde{M})^{-1}\Phi\ .$$

The next step, the construction of the FHL conjugate momenta $P_{x^{(0)},\mu}$, requires one to relate the time derivative of the effective links $\tilde{U}_i$, which are each composed of a sum of products of three fine links U_{ν_k} [according to Eq. (A4)], to the time derivative of single links on the FHL.

Concerning the straight part, we profit from the fact that the second term in Eq. (A7) is the Hermitian conjugate of the first; we can therefore restrict our calculation to the effective links $\tilde{U}_i$ and later reconstruct the Hermitian conjugate part. For the diagonal paths, the situation is technically more complicated because of the occurrence of negative direction vectors; cf., Table II. In order to obtain the convenient form of Eq. (6), we take the effective link $\tilde{U}_i(x^{(1)})$, pointing in a positive direction, for the very case when the picked $\dot{U}_{v_k}$ is pointing in a positive direction of the FHL. In the case where $\dot{U}_{v_k}$ would go into a negative direction, we use $\tilde{U}_i^{\dagger}(x^{(1)}-e_i^{(1)})$ because $\dot{U}_{v_k}$ then also points in a positive direction on the FHL. $\tilde{U}_i^{\dagger}(x^{(1)}-e_i^{(1)})$ is equivalent to $\tilde{U}_{-i}(x^{(1)})$, which corresponds to a path in a negative direction. In both cases we can reconstruct the missing Hermitian conjugate part as for the straight links.

We organize the $\dot{U}$'s in three classes (see Fig. 10): (1) $\dot{U}$'s "outgoing" from site $x^{(1)}$, (2) "Intermediate" $\dot{U}$'s which are not at all connected with a blocked site; (3) "ingoing" $\dot{U}$'s, the tip of which is in contact with a blocked site. The function $F_{x^{(0)},\mu}$ of Eq. (6) can now be written down explicitly. We distinguish the three classes:

$$F^{\text{out}}_{x^{(0)},\rho}=\sum_{l=1}^{7}\frac{\kappa}{\sigma}U_\mu(x^{(1)}+e_\rho^{(0)})U_\sigma(x^{(1)}+e_\rho^{(0)}+e_\mu^{(0)})P_{x^{(1)},i},\qquad x^{(0)}=x^{(1)},$$

$$F^{\text{in}}_{x^{(0)},\sigma}=\sum_{l=1}^{7}\frac{\kappa}{\sigma}P_{x^{(1)}-e_i^{(1)},i}U_\rho(x^{(1)}-e_i^{(1)})\times U_\mu(x^{(1)}-e_i^{(1)}+e_\rho^{(0)}),\quad x^{(0)}=x^{(1)}-e_\sigma^{(0)},\tag{A8}$$

$$F^{\text{inter}}_{x^{(0)},\mu}=\frac{\kappa}{\sigma}U_\sigma(x^{(1)}+e_\rho^{(0)}+e_\mu^{(0)})P_{x^{(1)},i}U_\rho(x^{(1)}),\qquad x^{(0)}=x^{(1)}+e_\rho^{(0)}.$$

$\sigma=6$ in the case of a diagonal path and 1 in the case of a straight path. The contributing paths for outgoing and ingoing $\dot{U}$'s are destinated by fixing ρ (σ). The contributions to a specified $F_{x^{(0)},\nu}$ can be read off Table III; there they are labeled by the index l. Concerning intermediate links, there are two directions to be specified. Each choice of ρ and σ corresponds to one definite $F_{x^{(0)},\mu}$. A bar again has the meaning of a minus sign; $\bar{i}$ denotes a negative path.

TABLE III. List of indices which specify $F_{x^{(0)},\nu}$ according to Eq. (A8).

Outgoing

ρ	1				2				3				4			
l	No.	μ	σ	i	No.	μ	σ	i	No.	μ	σ	i	No.	μ	σ	i
1	1	2	3	1	3	1	3	1	5	1	2	1	11	$\bar{1}$	2	2
2	2	3	2	1	4	3	1	1	6	2	1	1	12	2	$\bar{1}$	2
3	10	$\bar{4}$	$\bar{2}$	$\bar{2}$	9	$\bar{1}$	4	2	10	$\bar{4}$	$\bar{1}$	$\bar{3}$	17	1	$\bar{3}$	3
4	12	$\bar{2}$	$\bar{4}$	$\bar{2}$	10	4	$\bar{1}$	2	17	$\bar{1}$	$\bar{4}$	$\bar{3}$	18	$\bar{3}$	1	3
5	13	$\bar{3}$	4	3	22	$\bar{4}$	$\bar{3}$	$\bar{4}$	21	$\bar{2}$	4	4	23	$\bar{2}$	3	4
6	14	4	$\bar{3}$	3	24	$\bar{3}$	$\bar{4}$	$\bar{4}$	22	4	$\bar{2}$	4	24	3	$\bar{2}$	4
7	25	1	1	5	26	2	2	6	27	3	3	7	28	4	4	8

Ingoing

σ	1				2				3				4			
l	No.	ρ	μ	i	No.	ρ	μ	i	No.	ρ	μ	i	No.	ρ	μ	i
1	4	2	3	1	2	1	3	1	1	1	2	1	7	$\bar{1}$	2	2
2	6	3	2	1	5	3	1	1	3	2	1	1	9	2	$\bar{1}$	2
3	$\bar{7}$	$\bar{4}$	$\bar{2}$	$\bar{2}$	8	$\bar{1}$	4	2	15	$\bar{4}$	$\bar{1}$	$\bar{3}$	13	1	$\bar{3}$	3
4	$\bar{8}$	$\bar{2}$	$\bar{4}$	$\bar{2}$	11	4	$\bar{1}$	2	16	$\bar{1}$	$\bar{4}$	$\bar{3}$	15	$\bar{3}$	1	3
5	16	$\bar{3}$	4	3	19	$\bar{4}$	$\bar{3}$	$\bar{4}$	20	$\bar{2}$	4	4	19	$\bar{2}$	3	4
6	18	4	$\bar{3}$	3	20	$\bar{3}$	$\bar{4}$	$\bar{4}$	23	4	$\bar{2}$	4	21	3	$\bar{2}$	4
7	25	1	1	5	26	2	2	6	27	3	3	7	28	4	4	8

Intermediate

μ	1				2				3				4			
	ρ	No.	σ	i	ρ	No.	σ	i	ρ	No.	σ	i	ρ	No.	σ	i
	1	25	1	5	1	1	3	1	1	2	2	1	1	14	$\bar{3}$	3
	$\bar{1}$	7	4	2	$\bar{1}$	18	$\bar{4}$	$\bar{3}$	$\bar{1}$	8	2	2	2	3	3	1
	2	26	2	6	2	4	1	1	2	10	$\bar{1}$	$\bar{2}$	$\bar{2}$	11	$\bar{4}$	$\bar{2}$
	$\bar{2}$	19	4	4	$\bar{2}$	20	3	4	$\bar{2}$	5	2	1	3	6	1	1
	3	27	3	7	3	22	3	$\bar{2}$	$\bar{3}$	15	4	3	$\bar{3}$	23	$\bar{4}$	$\bar{4}$
	$\bar{3}$	16	1	3	4	17	$\bar{3}$	3	4	12	$\bar{1}$	2	4	24	$\bar{2}$	4
	4	28	4	8	$\bar{4}$	9	$\bar{2}$	$\bar{2}$	$\bar{4}$	21	$\bar{3}$	$\bar{4}$	$\bar{4}$	13	$\bar{1}$	$\bar{3}$

[1] M. Fukugita, S. Ohta, and A. Ukawa, Phys. Rev. Lett. **57**, 1974 (1988).

[2] K. Bitar, A. D. Kennedy, and P. Rossi, Phys. Lett. B **234**, 333 (1990).

[3] S. Duane, A. D. Kennedy, B. J. Pendleton, and D. Roweth, Phys. Lett. B **195**, 216 (1987).

[4] S. Gottlieb, W. Liu, D. Toussaint, R. L. Renken, and R. L. Sugar, Phys. Rev. D **35**, 2531 (1987).

[5] See, e.g., A. Ukawa, in *Lattice '89,* Proceedings of the International Symposium, Capri, Italy, 1989, edited by R. Petronzio *et al.* [Nucl. Phys. B (Proc. Suppl.) **17**, 118 (1990)].

[6] N. H. Christ, in *Lattice '90,* Proceedings of the International Symposium, Tallahassee, Florida, 1990, edited by U. M. Heller, A. D. Kennedy, and S. Sanielevici [Nucl. Phys. B (Proc. Suppl.) **20**, 129 (1991)].

[7] R. Gupta, C. Baillie, R. Brickner, G. Kilcup, A. Patel, and S. in *Lattice '90* [6], p. 385.

[8] F. Wilczek, Phys. Rev. Lett. **59**, 2397 (1987).

[9] S. Güsken, R. Gupta, K.-H. Mütter, A. Patel, K. Schilling, and R. Sommer, Nucl. Phys. **B314**, 63 (1989).

[10] Ph. de Forcrand, S. Güsken, R. Gupta, K.-H. Mütter, A. Patel, K. Schilling, and R. Rommer, Phys. Lett B **200**, 143 (1988).

[11] S. Güsken, R. Sommer, K.-H. Mütter, A. Patel, and K. Schilling, Phys. Lett. B **212**, 216 (1988); K. Schilling, in *Lattice '88,* Proceedings of the International Symposium, Batavia, Illinois, 1988, edited by A. S. Kronfeld and P. B. Mackenzie [Nucl. Phys. B (Proc. Suppl.) **9**, 389 (1989)]; S. Güsken, K.-H. Mütter, R. Sommer, A. Patel, and K.

Schilling, Nucl. Phys. **B327**, 763 (1989); S. Güsken, K.-H. Mütter, K. Schilling, R. Sommer, and A. Patel, Phys. Lett. B **227**, 266 (1989); K.-H. Mütter, in *Proceedings of Physics at HR67,* edited by M. Kormer (Forschungszentrum, Jülich, 1990), p. 245.

[12] R. Cordery, R. Gupta, and M. Novotny, Phys. Lett. **128B**, 425 (1983).

[13] S. Aoki, Phys. Rev. D **30**, 2653 (1984); Phys. Lett. B **190**, 140 (1987).

[14] I. M. Barbour, N.-E. Behill, P. E. Gibbs, G. Schierholz, and M. Teper, in *The Recursion Method and Its Applications,* edited by D. G. Pettifor and D. L. Weaire, Springer Series in Solid-State Sciences Vol. 58 (Springer, Berlin, 1985), p. 149.

[15] K. Bitar, A. D. Kennedy, R. Horsley, S. Meyer, and P. Rossi, Nucl. Phys. **B313**, 377 (1989).

[16] A. Ukawa, CERN Report No. CERN-TH-5245/88, 1988 (unpublished).

[17] M. Bochicchio, L. Maiani, G. Martinelli, G. C. Rossi, and M. Testa, Nucl. Phys. **B262**, 331 (1985).

[18] L. Maiani and G. Martinelli, Phys. Lett. B **178**, 265 (1986).

[19] M. Engeli *et al., Mitteilungen aus dem Institut für angewandte Mathematik* (Birkhäuser Verlag, Berlin, 1959), Vol. 8, p. 79.

[20] R. Setoodeh, C. T. H. Davies, and I. M. Barbour, Phys. Lett. B **213**, 195 (1988).

[21] J. Kogut and C. DeTar, Phys. Rev. D **36**, 2828 (1987).

[22] S. A. Gottlieb, J. Kuti, D. Toussaint, A. D. Kennedy, S. Meyer, B. J. Pendleton, and R. L. Sugar, Phys. Rev. Lett. **55**, 1958 (1985).

[23] R. Gupta, C. Baille, R. Brickner, G. Kilcup, A. Patel, and S. Sharpe, Phys. Rev. D **44**, 3272 (1991).

[24] J. Smit and J. C. Vink, Nucl. Phys. **B286**, 485 (1987).

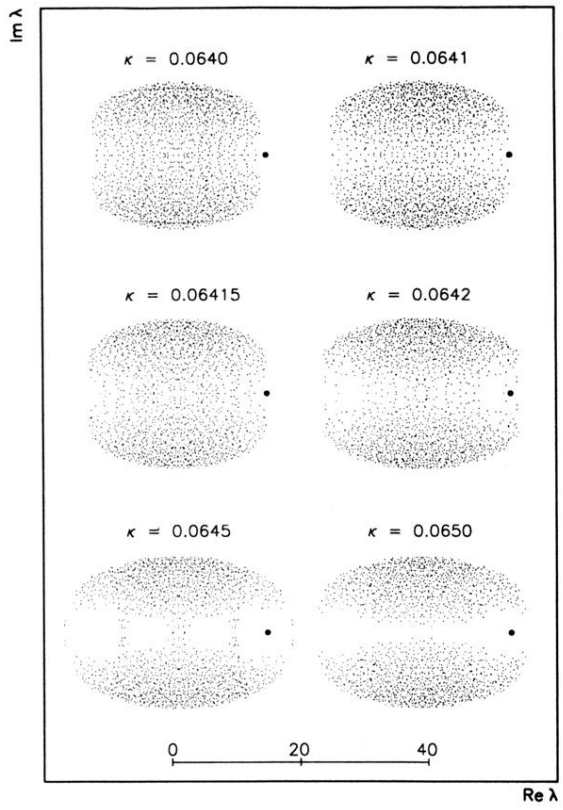

FIG. 5. Change in the eigenvalue distribution across the phase transition. Each picture is a typical representant borrowed from a series of configurations at equal κ. The bold point denotes the location of κ_c as obtained by extrapolation of $1/N_{CG}$ (Fig. 2). The scale drawn in is valid for both the abscissa and the ordinate.

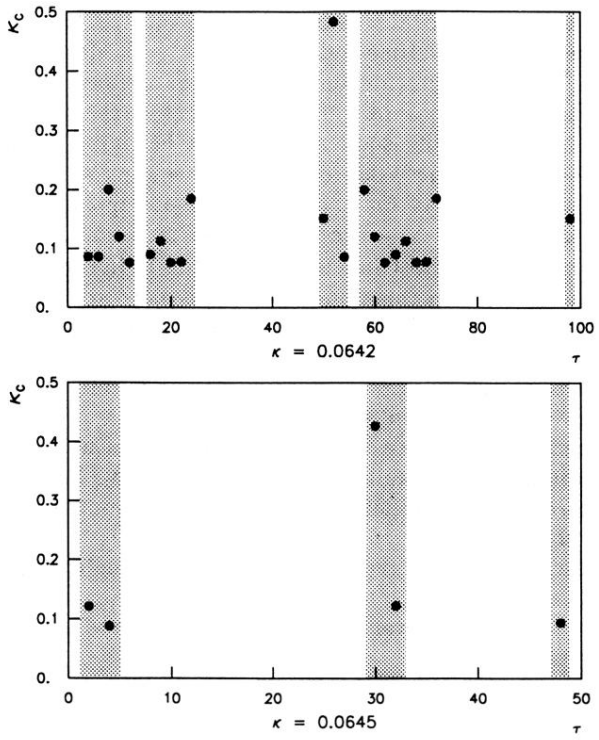

FIG. 6. Flip-flop behavior for $\kappa > \kappa_s$ on a 6^4 lattice. $1/\lambda^r_{\max}$ is plotted as function of the molecular-dynamics time τ for two values of κ. The shadows denote the regions where purely real eigenvalues of the fermion matrix occur.